

A Moving Grid Finite Element Method for the Simulation of Pattern Generation by Turing Models on Growing Domains

Anotida Madzvamuse,¹ Philip K. Maini,² and Andrew J. Wathen³

Received November 10, 2003; accepted (in revised form) March 8, 2004

Numerical techniques for moving meshes are many and varied. In this paper we present a novel application of a moving grid finite element method applied to biological problems related to pattern formation where the mesh movement is prescribed through a specific definition to mimic the growth that is observed in nature. Through the use of a moving grid finite element technique, we present numerical computational results illustrating how period doubling behaviour occurs as the domain doubles in size.

KEY WORDS: Moving meshes; moving grid finite elements; reaction–diffusion systems; Turing instability.

1. INTRODUCTION

It is more than half a century ago since the publication of the celebrated paper by Turing [40] on morphogenesis i.e. the development of patterns, shapes and structures found in nature. Turing demonstrated theoretically that a system of two reacting and diffusing chemical concentrations (termed morphogens) could give rise to spatial patterns in concentrations through a chemical instability process, now known as Turing diffusion-driven instability. The novelty of his idea was that by adding diffusion to a system of reaction equations with a stable homogeneous steady state

¹ Auburn University, Mathematics Department, 316A Parker Hall, Auburn, AL 36849, USA.
E-mail: madzval@auburn.edu

² Centre for Mathematical Biology, Mathematical Institute, University of Oxford, 24–29 St Giles', Oxford OX1 3LB, UK.

³ Oxford University Computing Laboratory, Wolfson Building, Parks Road, Oxford OX 13QD, UK.

solution, the system could become unstable and evolve to a non-uniform spatially varying steady state solution. In most physical systems, diffusion is by contrast a stabilising mechanism. Typical examples of biological applications of reaction–diffusion systems are: pattern formation in hydra [12], animal coat markings [27], butterfly wing pigmentation patterns [28], skeletal patterning in limb development [21] and shell pigmentation patterns [22] among many others. Experimental evidence supporting the Turing instability has been found in chemistry: the chlorite-iodide-malonic acid starch reaction (CIMA reaction) was the actual chemical reaction in which Turing patterns were first observed [8, 11]. Lengyel and Epstein [16], proposed a model for this reaction in which the chemical kinetics can be determined experimentally. It is now known that morphogens exist in biology but the whole issue of self-organisation via the Turing instability is highly controversial [4].

One of the major criticisms of Turing reaction-diffusion theory for pattern formation on fixed domains is the sensitivity of the patterns to initial conditions and the tight control of model parameter values needed [3]. However, by incorporating domain growth, we have shown that period doubling of patterns can occur [20]. These patterns are insensitive to initial conditions thereby enhancing the robustness of pattern selection.

In biological species, the role of domain growth in pattern formation has been well illustrated in the paper by Kondo and Asai [14] who show experimentally mode doubling in the circular patterns of the marine angelfish *Pomacanthus* as it grows. The juvenile *Pomacanthus*, which is less than 2 cm long, has three dorsoventral or vertical stripes; however once the fish grows to twice this body length, new stripes emerge between the original stripes so that the original wavelength is maintained. Painter *et al.* [30] and Crampin *et al.* [9] carried out theoretical and computational studies of the role of domain growth in pattern generation on regular domains (using finite difference schemes for their numerical simulations). However, their numerical method can not easily describe complicated and continuously deforming shapes. The applicability of the finite element methods to complicated domains is well known and there is growing realisation that continuously changing boundaries can be readily handled by moving grid implementations with few changes to the finite element methodology: at least this is true when grid motion is prescribed.

We employ the moving grid finite element method in a novel way which differs substantially from the classical moving finite element method [2,23]. The key aspect of the moving finite element method is the assumption that the solution and the nodal movement are unknown quantities which have to be solved for simultaneously. In most cases the solution of the partial differential equation and the nodal movement are expanded in

a piecewise linear finite element approximation space and then the least squares residual is minimised with respect to the time derivatives of the two unknown quantities. This method thus yields both the solution and the nodal movement simultaneously and directly in terms of the physical coordinates. However, the method requires regularisation to cope with potential singularities arising from the double minimisation of the solution and the nodal movement. Also crucially important is that mesh tangling is a real possibility and this could greatly reduce applicability. Our method however differs in that nodal movement is experimentally defined. This is a key advantage in that mesh tangling is therefore not an issue in our numerical computations. The mesh movement and the time discretisation of the PDE are intrinsically coupled. The boundary is deformed continuously in some prescribed fashion (in most cases to mimic biological experiments) and the internal mesh movement is achieved either via a specific definition or in some cases, where no such definition exists, via the spring analogy described by Blom [5].

In Sec. 2 we illustrate one derivation of reaction–diffusion systems on a continuously deforming domain. The model equations derived are solved via a moving grid finite element method by use of piecewise linear basis functions in two dimensions as shown in Sec. 3. In Sec. 4 we illustrate the application of the numerical method by computing numerical results on a continuously deforming square domain. Through a specific example we show computationally how period doubling of spots occurs with domain growth. Finally in Sec. 5 we present conclusions and some future directions in this research.

2. DERIVATION OF REACTION–DIFFUSION EQUATIONS ON A CONTINUOUSLY DEFORMING DOMAIN

Let $\Omega(t) \subset \mathbb{R}^2$ be a simply connected bounded growing domain at time $t \geq 0$ with its growing boundary $\partial\Omega(t)$. Also let $u(x(t), y(t), t)$ and $v(x(t), y(t), t)$ be the concentrations of two chemicals, known as morphogens, at position $(x(t), y(t)) \in \Omega(t) \subset \mathbb{R}^2$ at time $t \geq 0$.¹ Consider chemical concentration u (similarly for v), say. According to the law of mass balance, at time $t \geq 0$, the rate of change of the chemical u in $\Omega(t)$ is equal to the sum of its net flux, \mathbf{F}_1 , through the boundary $\partial\Omega(t)$ and the net production, f_1 , of the chemical within the domain. Therefore by the Divergence Theorem we have

$$\frac{d}{dt} \int_{\Omega(t)} u(x(t), y(t), t) \, d\Omega(t) = \int_{\Omega(t)} \left(-\nabla \cdot \mathbf{F}_1 + f_1(u, v) \right) \, d\Omega(t), \quad (2.1)$$

¹This can be generalised to the case of $n > 2$ chemicals.

where we take into account the limits of integration which are time dependent. The differential operator can not be passed through the integral straight away since the limits of integration are functions of time. We will refer to the grid deformation of a domain in analogy with a flowing fluid with the aim of preserving the classical terminology [9]. The Reynolds transport theorem states that

$$\frac{d}{dt} \int_{\Omega(t)} G(x(t), y(t), t) d\Omega(t) = \int_{\Omega(t)} \left(\frac{DG}{Dt} + G(\nabla \cdot \mathbf{a}) \right) d\Omega(t) \quad (2.2)$$

for any scalar or vector function $G(x(t), y(t), t)$ (see, for example [1]). Here DG/Dt is the material derivative of G and it represents the rate of change of G following the fluid, and $\mathbf{a}(x(t), y(t), t)$ is the flow velocity field i.e.

$$\frac{DG}{Dt} = \frac{\partial G}{\partial t} + \mathbf{a} \cdot \nabla G. \quad (2.3)$$

Applying the Reynolds transport theorem to Eq. (2.1) we have

$$\begin{aligned} \frac{d}{dt} \int_{\Omega(t)} u(x(t), y(t), t) d\Omega(t) &= \int_{\Omega(t)} \left(\frac{Du}{Dt} + u(\nabla \cdot \mathbf{a}) \right) d\Omega(t) \\ &= \int_{\Omega(t)} \left(\frac{\partial u}{\partial t} + \mathbf{a} \cdot \nabla u + u(\nabla \cdot \mathbf{a}) \right) d\Omega(t) \\ &= \int_{\Omega(t)} \left(\frac{\partial u}{\partial t} + \nabla \cdot (\mathbf{a}u) \right) d\Omega(t) \\ &= \int_{\Omega(t)} \left(-\nabla \cdot \mathbf{F}_1 + f_1(u, v) \right) d\Omega(t). \end{aligned} \quad (2.4)$$

This holds for any arbitrary domain $\Omega(t)$ and the integrands are continuous so we have

$$\frac{\partial u}{\partial t} + \nabla \cdot (\mathbf{a}u) = -\nabla \cdot \mathbf{F}_1 + f_1(u, v). \quad (2.5)$$

Assuming that the chemical flux of u follows Fick's law: $\mathbf{F}_1 = -D_1 \nabla u$, then (2.5) becomes

$$\frac{\partial u}{\partial t} + \nabla \cdot (\mathbf{a}u) = f_1(u, v) + D_1 \nabla^2 u, \quad (2.6)$$

and similarly for v we have

$$\frac{\partial v}{\partial t} + \nabla \cdot (\mathbf{a}v) = f_2(u, v) + D_2 \nabla^2 v. \quad (2.7)$$

Here, we have presented a general framework for considering domain growth which will allow for subsequent inclusion of a detailed description of the properties of specific tissues. The derivation is considered as a kinematic problem and no constitutive equations are proposed. It is simply assumed that the domain undergoes deformation and expansion resulting in the convection of material [10]. Combining (2.6) and (2.7) in vector form we obtain:

$$\frac{\partial \mathbf{u}}{\partial t} + \nabla \cdot (\mathbf{a} : \mathbf{u}) = \mathbf{f}(\mathbf{u}) + \mathbf{D} \nabla^2 \mathbf{u}, \tag{2.8}$$

where $\mathbf{a} : \mathbf{u} = (\mathbf{a} u, \mathbf{a} v)^T$. One form of non-dimensionalisation [26] leads to the generalised reaction–diffusion system

$$\frac{\partial \mathbf{u}}{\partial t} + \nabla \cdot (\mathbf{a} : \mathbf{u}) = \gamma \mathbf{f}(\mathbf{u}) + \mathbf{D} \nabla^2 \mathbf{u} \quad \text{in } \Omega(t) \tag{2.9}$$

with $\Omega(t)$ representing a time-dependent domain. In some situations the reaction term $\gamma \mathbf{f}(\mathbf{u})$ can be re-defined and more helpfully be written as $\gamma \mathbf{f}(\mathbf{u}) + \mathbf{P}_3(\mathbf{u})$ which leads to

$$\frac{\partial \mathbf{u}}{\partial t} + \nabla \cdot (\mathbf{a} : \mathbf{u}) = \gamma \mathbf{f}(\mathbf{u}) + \mathbf{P}_3(\mathbf{u}) + \mathbf{D} \nabla^2 \mathbf{u} \quad \text{in } \Omega(t), \tag{2.10}$$

where $\mathbf{P}_3(\mathbf{u}) = (p_3(u, v), q_3(u, v))^T$ with p_3, q_3 being cubic polynomials [17]. We define

$$\mathbf{u} = \begin{pmatrix} u \\ v \end{pmatrix}, \quad \mathbf{f} = \begin{pmatrix} f(u, v) \\ g(u, v) \end{pmatrix}, \quad \mathbf{D} = \begin{pmatrix} D_u & 0 \\ 0 & D_v \end{pmatrix}, \quad \text{and} \quad \mathbf{x} = (x(t), y(t)),$$

where u, v are the two chemical concentrations under investigation, f, g, p_3, q_3 are reaction kinetics. \mathbf{D} is the diffusion matrix (D_u and D_v are constant diffusion parameters) and γ is a scale parameter [26]. In Madzvamuse *et al.* [17] typical classical reaction kinetics are presented, including the Gierer–Meinhardt [12], the Thomas [38] and the Schnakenberg [35] models. In this paper we use only the Schnakenberg reaction kinetics with $\mathbf{P}_3(\mathbf{u}) = \mathbf{0}$ and

$$\begin{aligned} f(u, v) &= a - u + u^2 v, \\ g(u, v) &= b - u^2 v. \end{aligned} \tag{2.11}$$

Boundary conditions can be of Dirichlet type or of (homogeneous) Neumann type which describe zero-flux of u (or v) out of the boundary. Initial conditions are prescribed as small random perturbations about the uniform homogeneous steady state of the corresponding reaction systems.

3. THE MOVING GRID FINITE ELEMENT METHOD

Following Madzvamuse *et al.* [17], let $w \in H^1(\Omega(t))$ be a test function. Multiplying the u component in Eq. (2.10) by w leads to the following problem:

$$(u_t + \nabla \cdot (\mathbf{a}u), w) = \gamma(f, w) + D_u(\nabla^2 u, w) \tag{3.1}$$

for all $w \in H^1(\Omega(t))$ where

$$(u, w) = \int \int_{\Omega(t)} u w \, d\mathbf{x} \tag{3.2}$$

is the L_2 -inner product. Assuming that homogeneous Neumann boundary conditions are used, by Green's Theorem equation (3.1) reduces to finding $u \in H^1(\Omega(t))$ such that

$$(u_t + \nabla \cdot (\mathbf{a}u), w) = \gamma(f, w) - D_u(\nabla u, \nabla w) \tag{3.3}$$

for all $w \in H^1(\Omega(t))$. Here

$$\mathbf{a} = (\dot{x}, \dot{y})^T \tag{3.4}$$

represents the grid velocity. Therefore, we seek to find a solution $u \in H^1(\Omega(t))$ such that

$$(u_t, w) + (\dot{x}u_x + \dot{y}u_y, w) + (u \nabla \cdot \mathbf{a}, w) = \gamma(f, w) - D_u(\nabla u, \nabla w) \tag{3.5}$$

for all $w \in H^1(\Omega(t))$. Let u^h be a moving grid finite element approximation to u defined by

$$u^h = \sum_{j=1}^n U_j(t) \phi_j(\mathbf{x}, \xi(t)), \tag{3.6}$$

where $\xi(t)$ represents the finite element moving grid. Then the moving grid finite element approximation seeks to find $u^h \in V^h \subset H^1$ such that

$$(u_t^h, w) + (\dot{x}u_x^h + \dot{y}u_y^h, w) + (u^h \nabla \cdot \mathbf{a}, w) = \gamma(f, w) - D_u(\nabla u^h, \nabla w) \tag{3.7}$$

for all $w \in V^h \subset H^1(\Omega(t))$. The time-derivative of (3.6) can be expressed in two dimensions as [7,13]

$$\frac{\partial u^h}{\partial t} = \sum_{j=1}^n \left(\frac{dU_j}{dt} - \dot{x}_j u_x^h - \dot{y}_j u_y^h \right) \phi_j(\mathbf{x}, \xi(t)). \tag{3.8}$$

Without loss of generality, taking the test function to be $w = \phi_i$, $i = 1, \dots, n$, the above equation can be written as follows:

$$\sum_{j=1}^n \left(\frac{dU_j}{dt} (\phi_j, \phi_i) - (\dot{x}_j u_x^h \phi_j + \dot{y}_j u_y^h \phi_j, \phi_i) + (\dot{x}_j u_x^h + \dot{y}_j u_y^h, \phi_i) + \nabla \cdot \mathbf{a} (\phi_j, \phi_i) U_j \right) = -D_u \sum_{j=1}^n (\nabla \phi_j, \nabla \phi_i) + \gamma (f, \phi_i) \quad (3.9)$$

for all $i = 1, 2, \dots, n$. Similarly for v^h we have

$$\sum_{j=1}^n \left(\frac{dV_j}{dt} (\phi_j, \phi_i) - (\dot{x}_j v_x^h \phi_j + \dot{y}_j v_y^h \phi_j, \phi_i) + (\dot{x}_j v_x^h + \dot{y}_j v_y^h, \phi_i) + \nabla \cdot \mathbf{a} (\phi_j, \phi_i) V_j \right) = -D_v \sum_{j=1}^n (\nabla \phi_j, \nabla \phi_i) + \gamma (g, \phi_i). \quad (3.10)$$

Integrating over the whole domain gives rise to the following system of nonlinear ordinary differential equations:

$$M \dot{\mathbf{U}} - (P + Q) \mathbf{U} + (\bar{U}_x + \bar{U}_y) \mathbf{U} + \nabla \cdot \mathbf{a} M \mathbf{U} = -D_u K \mathbf{U} + \gamma F(\mathbf{U}, \mathbf{V}), \quad (3.11)$$

$$M \dot{\mathbf{V}} - (P + Q) \mathbf{V} + (\bar{V}_x + \bar{V}_y) \mathbf{V} + \nabla \cdot \mathbf{a} M \mathbf{V} = -D_v K \mathbf{V} + \gamma G(\mathbf{U}, \mathbf{V}), \quad (3.12)$$

where M is the mass matrix, K is the stiffness matrix, and P , Q , \bar{U}_x , \bar{U}_y , \bar{V}_x , \bar{V}_y are resultant matrices from domain growth. The terms $F(\mathbf{U}, \mathbf{V})$ and $G(\mathbf{U}, \mathbf{V})$ represent matrices derived from the nonlinear reaction kinetics. For example, for the Schnakenberg reaction kinetics (2.11) we have the following:

$$F(\mathbf{U}, \mathbf{V}) = a \mathbf{F} - M \mathbf{U} + C(\mathbf{U}, \mathbf{V}), \quad (3.13)$$

$$G(\mathbf{U}, \mathbf{V}) = b \mathbf{F} - C(\mathbf{U}, \mathbf{U}) \mathbf{V}, \quad (3.14)$$

where M is the mass matrix as before, \mathbf{F} is the force vector and $C(\mathbf{U}, \mathbf{V})$ is the linearised matrix from the $u^2 v$ term. Specific details of the integrations that give rise to these matrices can be found in Madzvamuse [20].

In all our simulations $\nabla \cdot \mathbf{a}$ is calculated from plausible growth functions or those derived from biological experiments and therefore is a known quantity (for example, see Sec. 4 for specific details). Finally we can re-write the system of nonlinear ordinary differential equations in compact form as follows:

$$M \dot{\mathbf{U}} + D_u K \mathbf{U} = (P + Q - \bar{U}_x - \bar{U}_y - \nabla \cdot \mathbf{a} M) \mathbf{U} + \gamma F(\mathbf{U}, \mathbf{V}), \quad (3.15)$$

$$M \dot{\mathbf{V}} + D_v K \mathbf{V} = (P + Q - \bar{V}_x - \bar{V}_y - \nabla \cdot \mathbf{a} M) \mathbf{V} + \gamma G(\mathbf{U}, \mathbf{V}). \quad (3.16)$$

3.1. Time-stepping

We have developed a variety of time-stepping methods to cater for different types of solutions to Eqs. (3.15) and (3.16). If the solutions are highly oscillatory with steep gradients, it becomes necessary to use higher order time-stepping schemes [32]. However for solutions with low frequencies such as those in this paper we implement a Picard Iteration method coupled with an Implicit Backward Euler finite difference scheme. This method allows us to take bigger time-steps than even those required for higher order time-stepping schemes. All the results in this paper are obtained by using this method. Also in all our simulations we use a fixed constant time step Δt . From a biological point of view, growth occurs on a very slow time-scale and hence it is plausible to assume that the difference between the transient solutions between two successive computational grids is negligible. This makes it possible to linearise the nonlinear terms in the reaction kinetics by assuming that the term \mathbf{U}^2 , for example, can be written as a product of $\mathbf{U}^m \mathbf{U}^{m+1}$ where \mathbf{U}^m is the known solution calculated from the previous time $m \Delta t$. At each time-step we do not need to apply a fixed iteration but simply use a single fixed iteration step. In previous work we have found this to be sufficient [17]. Once linearised the set of linear algebraic equations obtained are solved using a Preconditioned Generalised Minimum Residual Method. Preconditioners such as ILU(0), ILUT, ILUTP, ILUK and MILU(0) can be used with the method [33,34]. However, in all our simulations we have found that the simple ILU(0) preconditioner is adequate.

4. TWO-DIMENSIONAL MOVING GRID FINITE ELEMENT RESULTS

In this section, we show results for a given growth function. Let

$$\mathbf{x}(t) = (X(0)r(t), Y(0)s(t)) \quad (4.1)$$

define the grid movement where $X(0)$ and $Y(0)$ represent the initial x and y coordinates at time $t=0$. The functions $r(t)$ and $s(t)$ specify the rate of growth of the initial grid and satisfy $r(0) = s(0) = 1$ and $r(t), s(t) > 0$ for all positive time. Differentiating

$$\dot{\mathbf{x}} = X(0)\dot{r}(t), \quad \dot{\mathbf{y}} = Y(0)\dot{s}(t) \quad (4.2)$$

and from Eq. (4.1) we have

$$X(0) = \frac{x}{r(t)}, \quad Y(0) = \frac{y}{s(t)} \quad (4.3)$$

so that

$$\dot{x} = \frac{x}{r(t)} \dot{r}(t), \quad \dot{y} = \frac{y}{s(t)} \dot{s}(t). \quad (4.4)$$

Computing these relations with (3.4) we deduce that

$$\nabla \cdot \mathbf{a} = \frac{\dot{r}(t)}{r(t)} + \frac{\dot{s}(t)}{s(t)}. \quad (4.5)$$

Here we illustrate results for the exponential growth

$$r(t) = s(t) = e^{\rho t}. \quad (4.6)$$

Let us consider typical two-dimensional transient solutions for the Schnakenberg reaction kinetics with model parameter values $a = 0.1$, $b = 0.9$, $\gamma = 1.0$, $D_u = 1.0$ and $D_v = 0.01$. Figures 1–3 show results obtained by use of the exponential growth (4.6) with growth rate $\rho = 10^{-5}$. Homogeneous Neumann boundary conditions are applied to both chemical concentrations u and v . Initial conditions are prescribed as small random perturbations around the homogeneous steady state (1.0, 0.9) in the form of:

$$u = 1.0 \pm 10^{-3} \cos\left(\frac{14\pi x}{2}\right), \quad (4.7)$$

$$v = 0.9 \pm 10^{-3} \cos\left(\frac{14\pi x}{2}\right). \quad (4.8)$$

The initial mesh is computed using a Delaunay mesh generator software [25]. The mesh connectivity remains constant throughout the growth of the domain, mesh points are not added or removed during the growth process. All the numerical simulations are carried out on a typical mesh of approximately 4000 elements with approximately 2000 nodes. A fixed time step of $\Delta t = 0.025$ is used. The results obtained are independent of the structure of the mesh—regular and irregular meshes yield similar results. Similar results have also been obtained with finer meshes. The transient process settles down very quickly to being independent of initial conditions providing they are small perturbations about the uniform steady state. By incorporating growth, the final solutions obtained are robust to

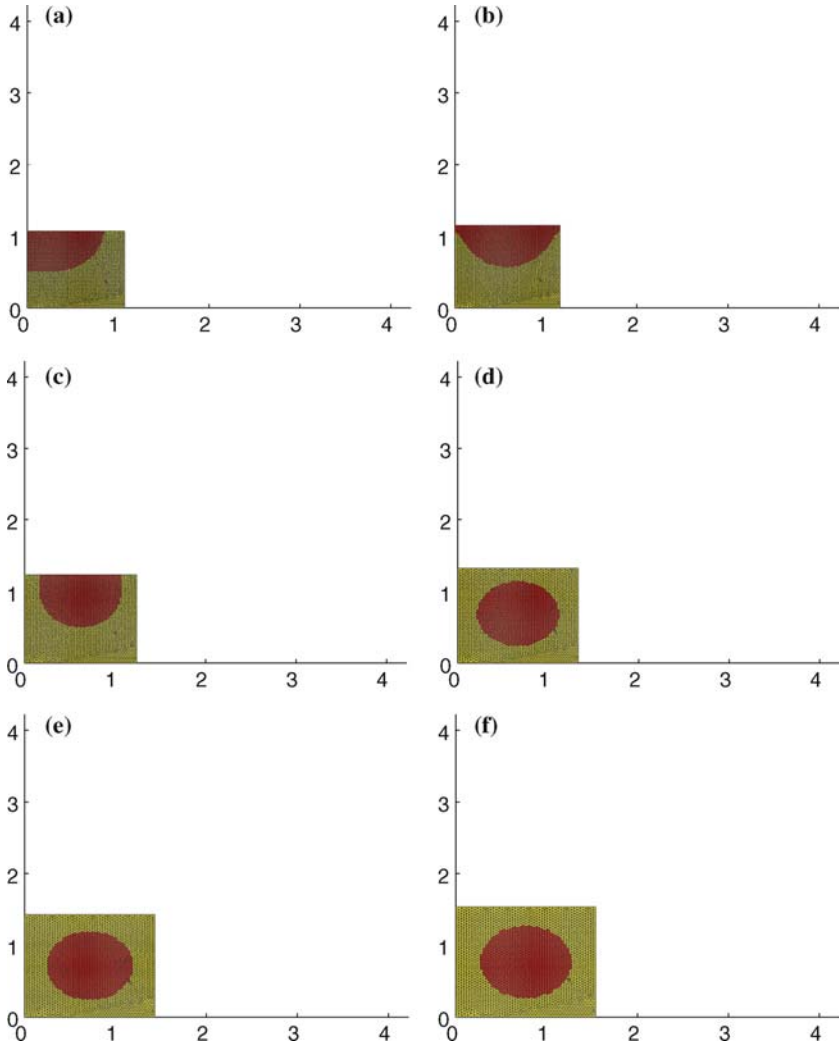


Fig. 1. Transient patterns generated by the Schnakenberg model as the unit square is grown along the diagonal line $x = y$ in the positive direction with growth rate (4.6). A spot pattern re-organises evolving to the centre of the square as the domain grows. Results shown correspond to the chemical concentration u : the v concentration profiles are 180-degrees out of phase with the u profiles.

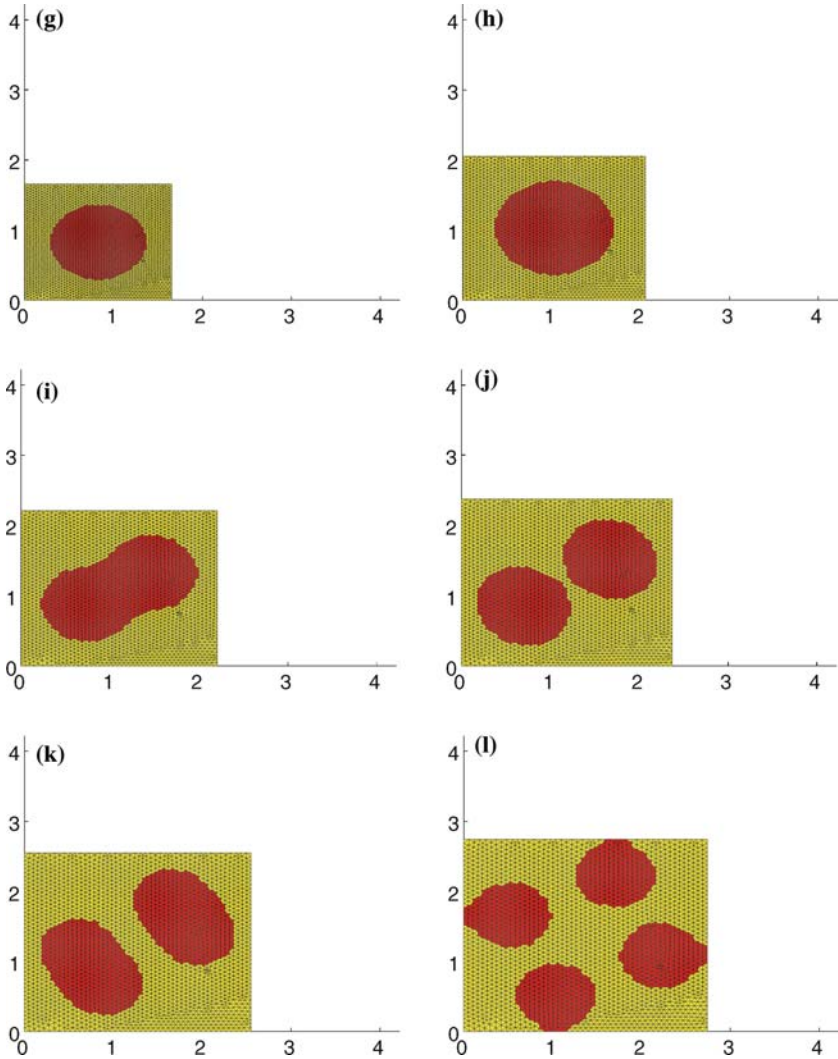


Fig. 2. Continuation of the simulation in Fig. 1. With further growth, the spot pattern enlarges in size and stretches along the diagonal to form a diagonal stripe pattern. This in turn splits into two. The spots align diagonally in the same fashion and split once more forming four spots. We observe that the spot doubled into two spots and then further doubles into four spots as the domain grows so that the side length is approximately twice that for the case when there is a single spot.

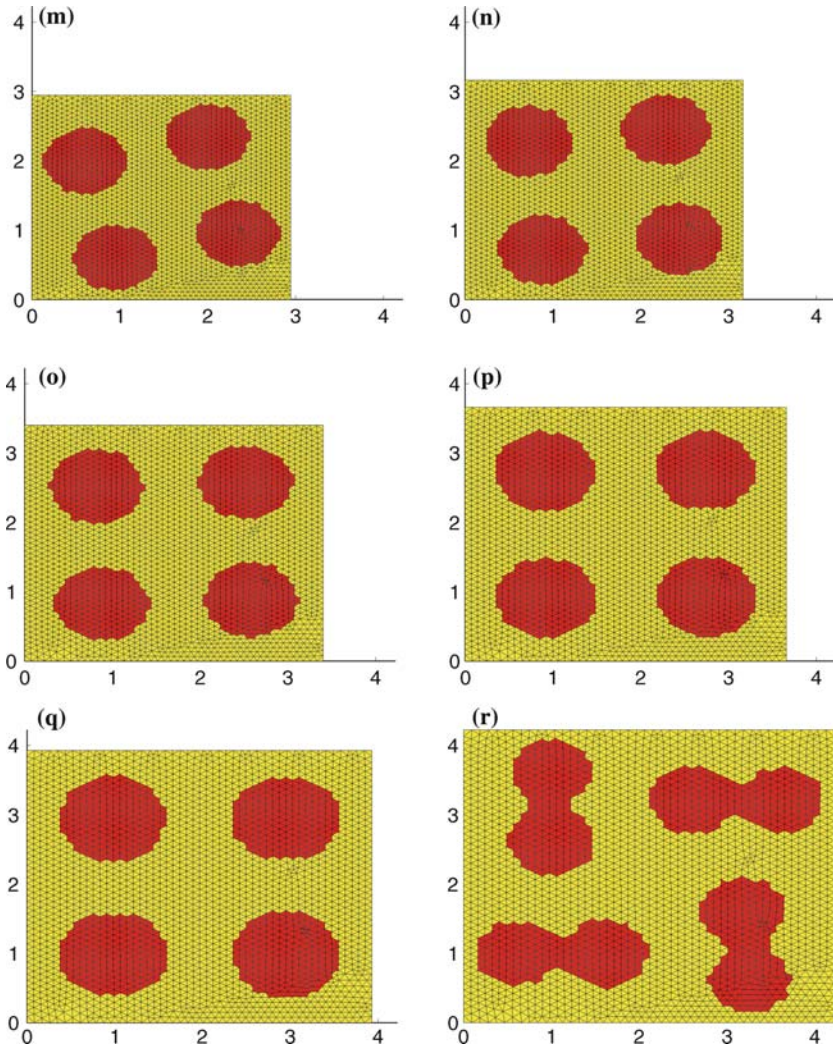


Fig. 3. Continuation of the simulation in Fig. 2. The spots re-orient to form a symmetrical pattern as the domain reaches approximately four times the size of the unit square. Finally we observe how eight spots are going to be formed with continuous growth of the square. Different random initial conditions have been applied without change in the numerical results, one realization of which is shown here.

initial conditions. In this case domain growth enhances the robust selection of patterning. These results agree with theoretical results derived by Crampin and others where they carried out studies on period doubling, peak insertion and splitting [9]. Period doubling of spots as the domain approximately doubles in size is observed as the domain grows. Interesting is the observation that a diagonal stripe (i) is first achieved before this splits into two spots (j). These in turn split into four spots which re-organise into a symmetrical pattern with further growth (l) – (q). The last picture shows how eight spots are going to be formed from four spots as the domain continues to grow (r). Although these results are only for illustrative purposes, from a biological point of view, period doubling of circular patterns is an interesting phenomenon and has been observed in the marine angelfish *Pomacanthus* [14].

We have illustrated results on growing two-dimensional squares, results on other polygons such as equilateral triangles, isosceles triangles, hexagonal and on irregular polygonal domains are shown in Madzvamuse *et al.* [17]. In all our simulations we observe numerical results that are independent of initial conditions.

5. CONCLUSIONS AND DISCUSSIONS

Experimentally it has been observed that domain growth plays a crucial role in the emergence of patterns in biological species (see, for example [14]). It is convenient to couple domain growth with reaction–diffusion systems and apply in a novel fashion the moving grid finite element method. This method differs from the classical moving finite element method [2,23] in that domain growth is prescribed, in most cases to mimic biological experiments. Although we have illustrated numerical results with a defined growth function (4.6) whereby the mesh velocity is prescribed throughout the domain, in some biological problems growth functions are unknown. Instead experiments provide discrete frames of domain growth and shape changes. For this nontrivial case, it becomes convenient to apply a spring analogy to calculate automatically the nodal positions of the internal mesh [5].

The phenomenon we observe of spot doubling on a growing domain is very similar to the process of self-replicating spots observed in computations on a fixed domain [31] and later experimentally [15].

We have found that in all our simulations transient solution on continuously growing domains are independent of initial conditions. In this paper we have shown a novel application of the moving grid finite element technique to solving a system of reaction-diffusion equations on a continuously growing domain. Intriguingly, we find that by using a finite differ-

ence approach to this problem the mode doubling transitions occur in a different sequence (Madzvamuse, in preparation). We believe that this may occur because the underlying model equations exhibit multiple solutions. This warrants further numerical and analytic investigation.

As part of this research we have developed a computer software package that can solve generalised Turing reaction–diffusion systems on continuously deforming one- and two-dimensional domains. This software has been applied to the study of growth patterns in bivalve ligaments [18,39], and on fixed domains to color pattern formation in the butterfly wing *Papilio dardanus* [19,29,36]. We are currently computing patterns on growing imaginal wing discs of butterflies. The software is freely available and downloadable from: <http://www.auburn.edu/~madzva1>.

ACKNOWLEDGMENTS

This work (AM) was carried out when the author was a research officer at Oxford University supported by the grant awarded to AJW and PKM from EPSRC Life Sciences Initiative (GR/R03914).

REFERENCES

1. Acheson, D. J. (1990). *Elementary Fluid Dynamics. Oxford Applied Mathematics and Computing Science*, Clarendon Press, Oxford.
2. Baines, M. J. (1994). *Moving Finite Elements, Monographs on Numerical Analysis*, Clarendon Press, Oxford.
3. Bard, J., and Lauder, I. (1974). How well does Turing's theory of morphogenesis work? *J. Theor. Biol.* **45**, 501–521.
4. Barinaga, M. (1994). Looking to development's future. *Science* **266**, 561–564.
5. Blom, J. F. (2000). Considerations of the spring analogy. *Int. J. Numer. Meth. Fluids.* **12**, 647–668.
6. Carlson, N. N., and Miller, K. (1998). Design and application of a gradient-weighted moving finite element code I: in one dimension. *SIAM J. Sci. Comput.* **19**(3), 728–765.
7. Carlson, N. N., and Miller, K. (1998). Design and application of a gradient-weighted moving finite element code II: in two dimensions. *SIAM J. Sci. Comput.* **19** (3), 766–798.
8. Castets, V., Dulos, E., Boissonade, J., and De Kepper, P. (1990). Experimental evidence of a sustained Turing-type equilibrium chemical pattern. *Phys. Rev. Lett.*, **64**(3), 2953–2956.
9. Crampin, E. J., Gaffney, E. A., and Maini, P. K. (2002). Reaction and diffusion on growing domains: Scenarios for robust pattern formation. *Bull. Math. Biol.* **61**, 1093–1120.
10. Crampin, E. J. (2000). *Reaction-diffusion Patterns on Growing Domains*, D Phil thesis, University of Oxford.
11. De Kepper, P., Castets, V., Dulos, E., and Boissonade, J. (1991). Turing-type chemical pattern in the chlorite–iodide–malonic acid reaction. *Physica D.* **49**, 161–169.
12. Gierer, A., and Meinhardt, H. (1972). A theory of biological pattern formation. *Kybernetik* **12**, 30–39.

13. Jimack, P. K., and Wathen, A. J. (1991). Temporal derivatives in the finite element method on continuously deforming grids. *SIAM J. Numer. Anal.* **28**(4), 990–1003.
14. Kondo, S., and Asai, R. (1995). A reaction–diffusion wave on the skin of the marine angelfish *Pomacanthus*. *Nature* **376**, 765–768.
15. Lee, K. J., McCormick, W. D., Ouyang, Q., and Swinney, H. L. (1994). Experimental observation of self-replicating spots in a reaction-diffusion system. *Nature* **369**, 215–218.
16. Lengyel, I., and Epstein, I. R. (1991). Modelling of Turing structure in the chlorite–iodide–malonic acid–starch reaction system. *Science* **251**, 650–652.
17. Madzvamuse, A., Maini, P. K., and Wathen, A. J., (2003). A moving grid finite element method applied to a model biological pattern generator. *J. Comp. Phys.* **190**, 478–500.
18. Madzvamuse, A., Maini, P. K., Wathen, A. J., and Sekimura, T. (2002). A predictive model for color pattern formation in the butterfly wing of *Papilio dardanus*. *Hiroshima Math. J.* **32**, 325–336.
19. Madzvamuse, A., Thomas, R. D. K., Maini, P. K., and Wathen, A. J. (2002). A numerical approach to the study of spatial pattern formation in the Ligaments of Arcoid Bivalves. *Bull. Math. Bio.* **64**, 501–530.
20. Madzvamuse, A. (2000). *A Numerical Approach to the Study of Spatial Pattern Formation*, D Phil thesis, University of Oxford.
21. Maini, P. K., and Solursh, M. (1991). Cellular mechanisms of pattern formation in the development of limb. *Int. Rev. Cytology.* **129**, 91–133.
22. Meinhardt, H. (1995). *The Algorithmic Beauty of Sea Shells*, Springer-Verlag, Heidelberg, New York.
23. Miller, K., and Miller, R. N. (1981). Moving finite elements. Part I. *SIAM J. Num. Anal.* **18**, 1019–1032.
24. Miller, K. (1981). Moving finite elements. Part II. *SIAM J. Num. Anal.* **18** 1033–1057.
25. Müller, J. D., Roe, P. L., and Deconinck, H. (1993). A frontal approach for internal node generation for Delaunay triangulation. *Int. J. Num. Meth. Fluids.* **17**(3), 241–256.
26. Murray, J. D. (1993). *Mathematical Biology*, Springer-Verlag, Heidelberg NY.
27. Murray, J. D. (1981). On pattern formation mechanisms for lepidopteran wing patterns and mammalian coat markings. *Phil. Trans. R. Soc. Lond.* **B(295)**, 473–496.
28. Nijhout, H. F. (1991). *The development and Evolution of Butterfly Wing Patterns*, Smithsonian Inst. Press, Washington, DC.
29. Nijhout, F. H., Maini, P. K., Madzvamuse, A., Wathen, A.J., and Sekimura, T. (2003) Pigmentation pattern formation in butterflies - experiments and models. *Comptes Rendus Biologies* **328**(8), 711–727.
30. Painter K. J., Maini, P. K., and Othmer, H. G. (1999). Stripe formation in juvenile *Pomacanthus* explained by a generalised Turing mechanism with chemotaxis. *Proc. Nat. Acad. Sci. USA.* **96**, 5549–5554.
31. Pearson, J. E. (1993). Complex patterns in a simple system. *Science* **261**, 189–192.
32. Ruuth, S. (1995). Implicit-explicit methods for reaction-diffusion problems in pattern-formation. *J. Math. Biol.*, **34**(2), 148–176.
33. Saad, Y. (1994). SPARSEKIT, a basic tool kit for sparse matrix computations. <http://www.users.cs.umn.edu/saad/>
34. Saad, Y. (1996). *Iterative Methods for Sparse Linear Systems*, PWS Publishing Co.
35. Schnakenberg, J. (1979). Simple chemical reaction systems with limit cycle behavior. *J. Theor. Biol.* **81**, 389–400.
36. Sekimura, T., Madzvamuse, A., Wathen, A. J., and Maini, P. K. (2000). A model for colour pattern formation in the butterfly wing of *Papilio dardanus*. *Proc. Roy. Soc. Lon.* **B(267)**, 851–859.

37. Sun, W., Tang, T., Ward, J. M., and Wei, J. (2003). Numerical challenges for resolving spike dynamics for two reaction-diffusion systems. *Stud. Appl. Math.* **111**, 41–84.
38. Thomas, D. (1975). Artificial enzyme membrane, transport, memory and oscillatory phenomena. In *Analysis and Control of Immobilised Enzyme Systems* Thomas, D., and Ker-venez, J.-P., (eds.), Springer Verlag, Berlin, Heidelberg, New York pp.115–150.
39. Thomas, R. D. K., Madzvamuse, A., Maini, P. K., and Wathen, A. J. (2000). Growth patterns of noetiid ligaments: implications of developmental models for the origin of an evolutionary novelty among arcoid bivalves. In *The Evolutionary Biology of the Bivalvia*, Harper, E. M., Taylor J.D., and Crame, J. A., (eds.), Geological Society Special Publication, **177**, 289–279.
40. Turing, A. M. (1952). The chemical basis of morphogenesis. *Phil. Trans. Roy. Soc. Lond.* **B** (237), 37–72.